Distribution of the Surfactant-Associated Protein C within a Lung Surfactant Model Film Investigated by Near-Field Optical Microscopy

A. Kramer,* A. Wintergalen,† M. Sieber,† H.J. Galla,† M. Amrein,‡ and R. Guckenberger*
*Max-Planck-Institut für Biochemie, D-82152 Martinsried, Germany; †Institut für Biochemie and ‡Institut für Medizinische Physik und Biophysik, Westfälische Wilhelms-Universität, D-48149 Münster, Germany

ABSTRACT Lung surfactant films at the air/water interface exhibit the particularity that surfactant molecules are expelled from the surface monolayer into a surface associated multilamellar phase during compression. They are able to re-enter the surface film during the following expansion. The underlying mechanism for this behavior is not fully understood yet. However, an important role is ascribed to the surfactant-associated protein C (SP-C). Here, we studied a model lung surfactant, consisting of dipalmitoylphosphatidylcholine (DPPC), dipalmitoylphosphatidylglycerol (DPPG), and SP-C, by means of scanning near-field optical microscopy (SNOM). Attaching a fluorescent dye to the protein allowed the localization of its lateral distribution at various surface pressures with high resolution. At an early stage of compression, the film appears demixed into a pure lipid phase and a protein-enriched phase. Within the latter phase, protein aggregations are revealed. They show a uniform density, having three times the fluorescence intensity of their surroundings. Across the phase boundary between the lipid phase and the protein-rich phase, there is a protein density gradient rather than an abrupt border. When the film is highly compressed, we observe the formation of multilamellar structures that are fluorescent. They are often surrounded by a slightly fluorescent monolayer. The fluorescence of the multilayer stacks (i.e., the protein content per unit area) is proportional to the height of the stacks.

INTRODUCTION

Pulmonary surfactant is a surface active substance present at the air/liquid interface of all air-breathing animals. It is secreted by alveolar type II cells. They form the outer cellular interface of the alveoli, together with other epithelial cells and macrophages. In the alveolar hypophase, the thin water layer covering the epithelial cells, the surfactant forms vesicles or tubular myelin. At the air/liquid interface it is spread as a mixed lipid-protein film. The presence of this layer is a prerequisite for a proper function of the lung because it reduces and adapts the surface tension of the interface dynamically to the varying surface area of the alveoli during breathing.

Pulmonary surfactant is composed mainly of dipalmitoylphosphatidylcholine (DPPC), phosphatidylglycerols (PGs), and proteins, besides other lipids, fatty acids, and cholesterol. Of the four surfactant associated proteins, SP-B and SP-C are extremely hydrophobic and, therefore, assumed to be particularly important in determining the surface active properties of pulmonary surfactant.

One possible function of the SP-C was recently illustrated by a molecular model based on results obtained from fluorescence light microscopy and scanning force microscopy of a model surfactant (Amrein et al., 1997; Galla et al., 1998). According to this model, the lung surfactant exists in two forms at the air/water interface of the lung: on the one hand, there is a monolayer consisting mainly of lipids; on the other hand, there are lipid multilayer stacks in close contact to the monolayer that contain most of the SP-C. The multilamellar phase forms upon film compression (i.e., exhalation) and acts as a surface-associated reservoir. Upon expansion of the film (i.e., inhalation), the lipids respread from this reservoir to the air/water interface. Thus, a fully covered interfacial surface and a permanently low surface tension is ensured. The assembly and disassembly, respectively, of the multilayer stacks during the breathing cycle is mediated by the SP-C. This function may result in part from the perfect fit of the hydrophobic α-helix of the protein within the hydrophobic moiety of a lipid bilayer. The positively charged amino acid residues in the head group of the peptide and the negatively charged lipid head groups may further stabilize the lipid-protein interaction.

The work presented here reveals the relation of the local SP-C content and the film topology at high spatial resolution by scanning near-field optical microscopy (SNOM) and simultaneous shear-force microscopy. By labeling the protein SP-C with a fluorescent dye, we chose the most direct way to localize the protein within the complex structure of the phase-separated films. The varying protein distribution within the film at various states of surface pressure in combination with the according film topology turns out to be of particular interest. It further elucidates the mechanism of how the SP-C molecule mediates the lipid exclusion from and integration into the surfactant monolayer.

Received for publication 18 June 1999 and in final form 20 October 1999.
Address reprint requests to Axel Kramer, Physikalische Chemie ETH Zürich CH-8092 Zürich, Switzerland. Tel.: 0041-1-632 7905; E-mail: kramer@phys.chem.etha.ch.

0006-3495/00/01/458/08 $2.00

MATERIALS AND METHODS

Materials

1,2-Dipalmitoyl-sn-glycero-3-phosphocholine (DPPC) and 1,2-Dipalmitoyl-sn-glycero-3-(phospho-rac-(1-glycerol)) (DPPG) were obtained from

Avanti Polar Lipids Inc. (Alabaster, AL) and were used without further purification. 7-Amino-3-((((succinimidyl)oxy)carbonyl)methyl)-4-methylcoumarin-6-sulfonic acid (AMCA-S-SE) was purchased from Molecular Probes (Eugene, OR). A recombinant form of the human surfactant protein C (SP-C) with two phenylalanines exchanged for the cysteines at position 4 and 5 and an isoleucine exchanged for the methionine at position 32 with the sequence GIPFFPVHLKRLLIVVVVVVLIVVVIVGALLIGL was a generous gift from Byk-Gulden Pharamceuticals (Konstanz, Germany). The identity was checked by electro-spray ionization mass spectrometry (ESI-MS). A molecular mass of 3618 Da confirmed the given structure. All solvents were HPLC grade and obtained from Merck (Darmstadt, Germany).

Synthesis of AMCA-S-labeled SP-C

Purified, recombinant SP-C was labeled with AMCA-S-SE by the following method. One milligram of the protein was dissolved in 1 ml of $CHCl_3/CH_3OH$ (1:1, vol:vol). After addition of a fourfold molar excess of AMCA-S-SE in $CH_3OH/CHCl_3$/DMF (2:1:1, vol:vol:vol; c = 5, 1 mM) and 200 μl of triethylamine, the solution was vortexed for 24 h at 25°C. The AMCA-S labeled SP-C was purified via reversed phase HPLC using the column Grom Sil C4 (Grom, Herrenberg, Germany). The probe was eluted with a linear gradient of H_2O (0.1%TFA)/$CH_3CHOHCH_3$ (0.1% TFA). ESI-MS was applied to determine the amount of labeled SP-C (SP-C-AMCA-S). The mass spectrum showed a peak corresponding to monolabeled protein with a yield of 96%.

Due to the small size of the attached dye group, changes in the surface properties of the protein were not expected. Film balance measurements resulted in no significant differences between the isotherms, either of the pure protein or of the lipid/protein mixtures.

Film deposition

For Langmuir-Blodgett transfer, the films were prepared on a film balance (Lauda-Königshofen, Germany) with an operational area of 925 cm^2. All molecular area/surface pressure measurements were performed at 20 ± 1°C on a pure water subphase (Milli-Q_{185}Plus, Millipore GmbH, Eschborn, Germany). The film composition was DPPC/DPPG (molar ratio 4:1) and SP-C-AMCA-S (0.4 mol%). Monolayers were formed by spreading aliquots of lipid/SP-C-AMCA-S mixtures directly from a $CHCl_3/CH_3OH$ (1:1, vol:vol) solution onto the surface. After the solvent was allowed to evaporate for 10 min, the compression was started with a rate of 0.03 nm^2 per molecule and minute.

For transfer the films were equilibrated to a well defined pressure (± 1 mN/m). Cleaned glass slides with a thickness of 0.17 mm were plunged through the surface at maximum speed of the deposition system (300 mm/min) until about 4 cm^2 of the slide were immersed in the subphase. The films were deposited on the upstroke (2 mm/min). In order to retain the physical state of the film during transfer, the film balance was normally operated in constant pressure mode. Completeness of transfer was checked by examination of the transfer ratio. Only samples exhibiting at least 95% transfer were considered. In case of film pressures of 50 mN/m (plateau region), due to the high compressibility of the film, the area of the film balance was reduced constantly during transfer according to the deposition rate. A direct test of completeness of transfer was not possible in this case. Therfore, the deposition was additionally checked by fluorescence light microscopy (Olympus BX-FLA light microscope, Olympus, Hamburg, Germany). Only films exhibiting a similar pattern before and after transfer were used in this study. If film transfer was successful according to the conditions described above, independent samples observed by near-field methods always showed similar structures.

Instruments

The mixed lipid-protein films were imaged with a home-built instrument, capable of far-field light microscopy, shear-force microscopy, and scanning near-field optical microscopy (Kramer et al., 1998). The instrument is mounted on a conventional inverted fluorescence microscope (Diaphot TMD Nikon, Düsseldorf, Germany). UV light of an Ar^+ laser (Model 2020–5S, Spectra Physics, Darmstadt, Germany) operating at the lines 335 nm, 351 nm, and 364 nm is fed into a special UV optical quartz fiber (AS10/125UVA, FiberTech, Berlin, Germany) which is tapered at the other end and Cr/Al-coated from the side (Betzig et al., 1991). The very low tip-sample separation during the scanning across the sample is kept constant by a tuning fork shear-force feedback system (Karrai and Grober, 1995). Exploiting this feedback signal, we are able to record a topography image simultaneously with the fluorescence image. The fluorescence is collected via the far-field optical system of the conventional microscope. For that reason a special UV objective with low autofluorescence had to be used (Fluorit 40×, 0.85 NA, Nikon). To separate the fluorescence from the excitation light we used a longpass filter (BA 400, Nikon). An avalanche photodiode served as sensitive detector with single photon counting capability (SPCM-PQ 200, EG&G, Gaithersburg, MD). Single molecule fluorescence detection efficiency was reached in the visible regime. However, with dyes excited in the UV the signal-to-background ratio decreased by a factor of about 20, due to autofluorescence of the tip coating. In order to keep the photobleaching of the dye molecules at a minimum, the sample was illuminated only during the backward scan with an image size of 128 × 128 pixel (except Fig. 3 *b*, 256 × 256 pixel).

The optical resolution of the microscope is determined mainly by the SNOM tip. For the investigations presented here we used a tip that was characterized after the lung surfactant measurements. Scanning the tip across a sharp metallic edge resulted in a transmission increase from 10 to 90% within a distance of 180 nm, representing a measure for the optical resolution attained.

RESULTS

The molecular area/surface pressure isotherm of the model lung surfactant consisting of DPPC:DPPG (4:1) and 0.4 mol% SP-C is shown in Fig. 1, along with the points on the

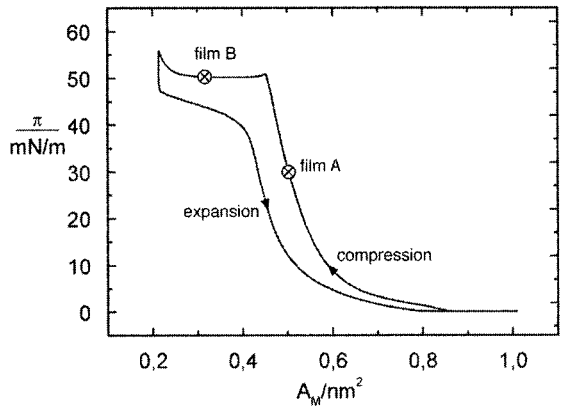

FIGURE 1 Molecular area/surface pressure isotherm of the lipids DPPC/DPPG (molar ratio 4:1) and the protein SP-C (0.4 mol%) on a water subphase at room temperature. The plateau formed at high surface pressure indicates the exclusion of material from the monolayer. The process of material exclusion is fully reversible indicated by the fact that a second compression of the film after expansion leads only to a neglectable shift of the isotherm to smaller molecular areas (von Nahmen et al., 1997b). The crosses in the isotherm mark the pressure at which the films used for investigation were transferred onto a glass coverslip. Film A was transferred at a pressure of 30 mN/m and film B in the plateau of the isotherm, respectively.

isotherm marking the state of the film at which the investigated films were transferred onto solid substrates (marked with a cross). Film A was transferred at a film pressure where it was still a monolayer (30 mN/m). Film B was taken at a state where the multilamellar phase, typical for the system investigated here, had already taken shape, in the plateau region of the molecular area/surface pressure isotherm.

In order to perform structural studies with the SNOM and the scanning force microscopy (SFM), the films were equilibrated at the respective state. They were then transferred onto glass coverslips via the Langmuir-Blodgett technique. Only those supports revealing a transfer ratio of more than 95% were used for further investigation. Fig. 2 shows the fluorescence and topography of film A recorded simultaneously with the SNOM. The shear-force topography image (Fig. 2 *a*) basically shows a smooth surface, being indicative of a monolayer on the glass surface. In the fluorescence image (Fig. 2 *b*) there are round dark domains embedded in a bright background. These large scale features of Fig. 2 *b* are in good agreement with conventional fluorescence light micrographs of similar specimens (Perez-Gil et al., 1992; von Nahmen et al., 1997b). Perez-Gil et al. and von Nahmen et al. described the dark domains as a pure lipid phase in the liquid condensed (LC) state, and the bright interspace as a phase containing both lipid and protein in a liquid expanded (LE) state. This was later confirmed by a qualitative analysis of the chemical composition of different film domains by laterally resolved time-of-flight secondary ion mass spectrometry (Galla et al., 1998). As is evident from Fig. 2 *b*, the bright LE phase, which appears homogeneous in a conventional light microscope (Amrein et al., 1997), actually exhibits a notable contrast in the SNOM image. There are very bright domains with sizes of 0.5 to 1 μm, embedded in a lesser fluorescent surrounding. Even domains as small as 100 to 200 nm are revealed (Fig. 2 *b*, *left*). Because it is directly the SP-C that carries the fluorescent dye, the locally varying brightness in the fluorescence image may directly be attributed to the local protein concentration. Hence, the bright domains are areas of high protein density. The information is obtained quantitatively from an intensity profile across such a domain (Fig. 2 *c*). The distinct plateau indicates a uniform fluorescence within the domain with a signal three times as high as that of the surroundings. In terms of protein density, the factor of three has to be considered as a lower limit. This is because the dense packing of the proteins within these regions likely leads to quenching of the fluorescence (von Nahmen et al., 1997b; Galla et al., 1998). Close to the pure lipid phase, the fluorescence intensity and, hence, the protein density gradually diminish over a distance of 0.5 to 0.8 μm.

For a discussion, we compare in Fig. 3 the results above to an earlier SFM study on films of similar composition prepared on mica (Amrein et al., 1997). Note that Fig. 3 *a* was not recorded by the SNOM, but by a home-built SFM.

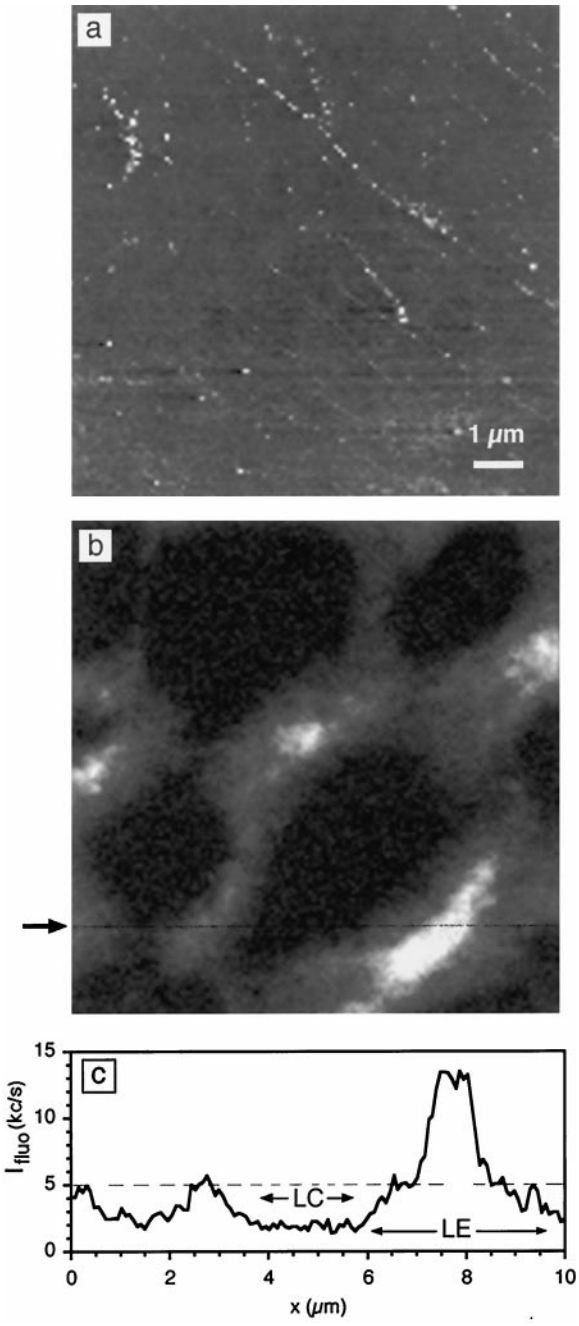

FIGURE 2 Simultaneously recorded topography (*a*) and near-field fluorescence images (*b*) of film A (see Fig. 1). The shear force image (*a*) shows a smooth monolayer surface, except for some small protrusions. In image (*b*) bright areas are due to the fluorescence of the dye-labeled SP-C. Consequently, it directly reflects the local protein distribution. The dark, round-shaped domains are attributed to a pure lipid phase of DPPC and DPPG in a liquid condensed state. The fluorescent region shows a strong contrast, indicating significant variations in the local protein concentration. (*c*) Intensity profile across a protein-rich domain in *b* (*arrow*). The fluorescence exhibits a plateau, suggesting a uniform SP-C concentration within this domain. The surrounding phase shows a three times weaker signal at a quasi-constant level (dashed), decreasing finally toward the LC phase. Excitation power: 3.7 nW, background fluorescence: 1.8 $\pm$ 0.3 kc/s, pixel integration time: 38 ms. Image grayscales (linear): height, 0–7 nm; fluorescence, 1.3–13.5 kc/s.

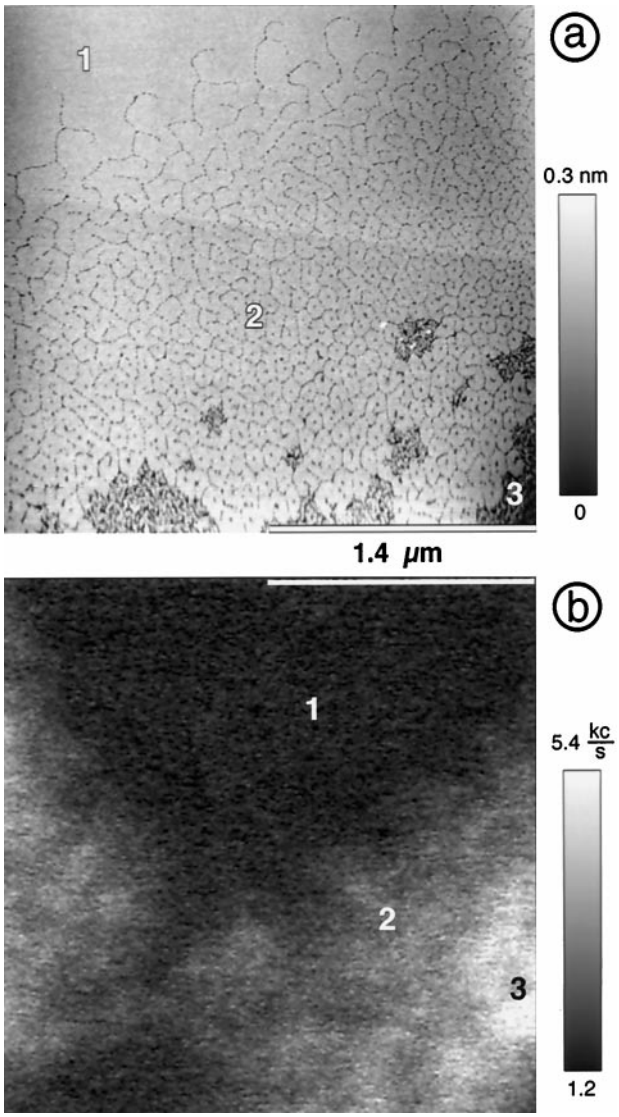

FIGURE 3 (*a*) Topography at the domain boundary region of a lipid LC patch of film A, recorded by scanning force microscopy (SFM). Three zones of different structure are discernible: a smooth one, assumed to be the pure lipid LC phase (zone 1); one with slightly reduced height and increased roughness (zone 3); in between an intermediate region with filamentous structures (zone 2). (*b*) Near-field fluorescence image (SNOM) of a different but equivalent sample compared to (*a*). The sample region is as in (*a*) a border region of a lipid LC patch. The corresponding shear-force image is not shown, since the topographical structures are not as evident as in the SFM image. The fluorescence micrograph allows to associate areas of different intensity to the above mentioned zones of the SFM image, thus confirming assumptions made previously (Amrein et al., 1997). Excitation power, 2.3 nW; background fluorescence, 1.5 ± 0.3 kc/s; pixel integration time, 10 ms.

This micrograph shows the border region of a lipid patch (corresponding areas appear dark in Fig. 2 *b*) and the protein containing phase. The morphology was classified by three different zones: a flat area (zone 1), an intermediate zone with a filamentous structure (zone 2), and a region of patches with slightly reduced height (zone 3). As a result of a detailed discussion, the smooth region was interpreted as a pure lipid phase (*top left*) and the more structured phase as a region rich in protein, with distinct patches of very high protein density (*bottom*). This interpretation is now supported by the comparison of the SFM results with the current SNOM investigation. Fig. 3 *b* shows a SNOM fluorescence image of a different but equivalent sample (same film composition, same transfer pressure) at a border region similar to that shown in Fig. 3 *a*. Bright fluorescent domains (*bottom right*) can be associated with the low islands (zone 3) observed in Fig. 3 *a*. They are surrounded by a region of constant fluorescence (zone 2), which then diminishes toward the nonfluorescent area (zone 1) on a length scale of typically 500 to 800 nm. Because in the SNOM image the fluorescence is a direct indication of SP-C concentration, we now can attribute zone 3 to the protein-rich area with the highest density, surrounded by a phase with a protein concentration at least three times lower (zone 2), finishing with a fringed edge, which penetrates into the flat areas (zone 1). In an independent experiment using secondary ion mass spectrometry this zone was identified as a pure lipid LC phase (Galla et al., 1998). Note that the width of the intermediate phase (zone 2) appears shortened in the SNOM image in comparison with the SFM topographical image. This is probably because the detection efficiency of the SNOM in the UV is not at the single molecule level. Hence, the fluorescence contribution is concealed by the background signal in the fluorescence image.

Fig. 4 shows the topography and fluorescence map of film B, transferred in the plateau region of the molecular area/surface pressure isotherm (Fig. 1). In this state of the film, there is a lamellar phase in coexistence with the monolayer phase in the presence of SP-C (von Nahmen et al., 1997a). In order to elucidate the formation of the lamellar phase, the combined fluorescence and topographical imaging performed in this study seems to be particularly helpful, because it allows localization of the peptide within the complex film structure. The film topography (Fig. 4 *a*) reflects what has been found in former studies: a smooth surface intersected by protrusions. They are the higher the more the film has been compressed before the transfer. The fluorescence image (Fig. 4 *b*) shows that regions of strong fluorescence directly correlate with high protrusions. Note that the gray scale of the fluorescence image is chosen logarithmic in order to emphasize regions with a weaker signal. Thereby, fluorescence from the monolayer in close proximity to the protrusions is revealed; i.e., a protein reservoir is present in the monolayer near the excluded material. Furthermore, this region exhibits very small, low protrusions (Fig. 4 *a*), probably the first sign of the beginning exclusion of material from the monolayer.

A higher magnification image (Fig. 5) shows that the protrusions are actually composed of the known lamellae, each about 5 to 6 nm in height. Again, a high fluorescence intensity is observed in regions where there are protrusions

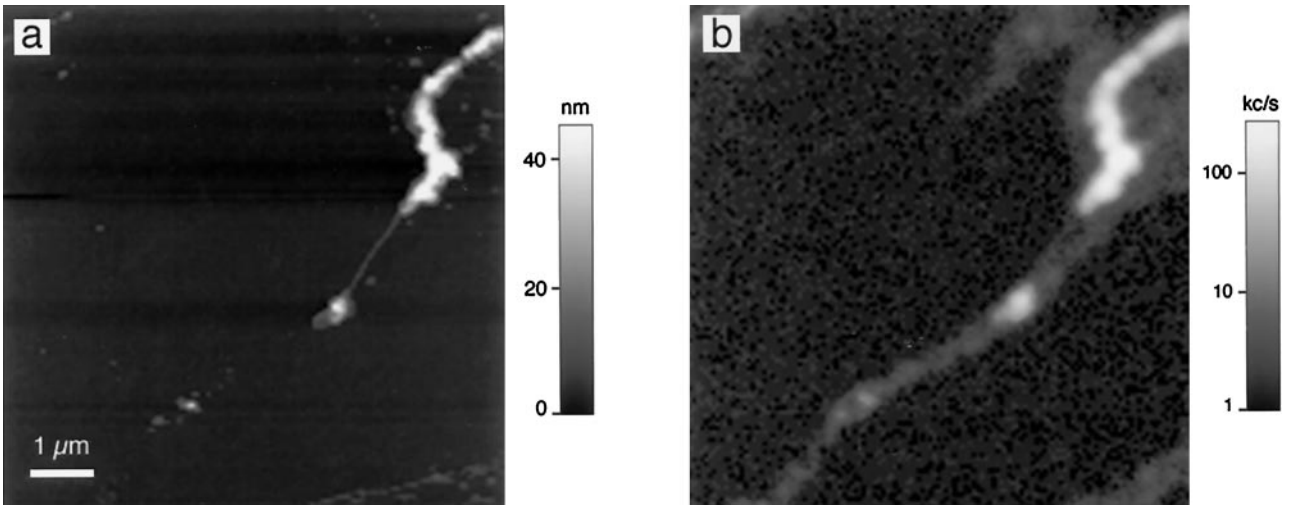

FIGURE 4 Simultaneously recorded topography (*a*) and near-field fluorescence image (*b*) of a film, transferred at the pressure plateau of the isotherm (film B, see Fig. 1). The topography image shows a smooth monolayer beside protrusions of up to 50 nm in overall height (*top right*) and smaller ones of 5–6 nm height. The SNOM fluorescence image (*b*), reflecting the protein distribution, exhibits the highest signal exactly at places where the highest protrusions are situated. Note that there is still protein in the associating monolayer, reflected by a weak fluorescence signal. The fluorescence gray scale is logarithmic. Excitation power, 5.7 nW; background fluorescence, 3.0 ± 0.6 kc/s; pixel integration time, 38 ms.

(Fig. 5 *b*). As in Fig. 4, monolayer fluorescence around the lamellae would be seen, if it were displayed in a logarithmic gray scale.

In order to get quantitative information about the protein content in the multilayer lamella, a correlation between fluorescence and topography was made (Fig. 6). The plot in Fig. 6 shows the results of a quantitative analysis of Fig. 5, revealing the relation between the fluorescence and the height of the multilayers. Only protrusions with a reasonable size (denoted by *crosses* in Fig. 5) were included in the analysis to ensure the full fluorescence contribution of each layer under the tip. The monolayer fluorescence is included in the analysis and is denoted by an open square in Fig. 6. The data points of the protrusions (*squares*) reflect a linear dependence of the fluorescence with the height of the multilayer stacks, stressed by the fit in Fig. 6. Hence, the volume density of the proteins in the protrusions appears to be constant. This leads to the conclusion that the formation

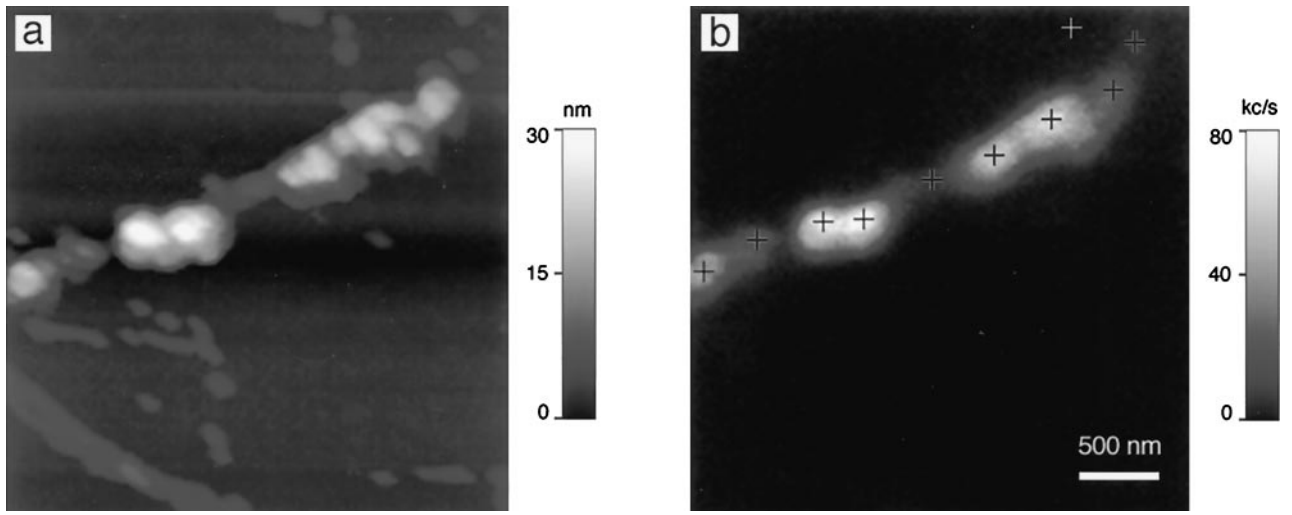

FIGURE 5 Topography (*a*) and near-field fluorescence image (*b*) of film B (3.1 μm × 3.1 μm). The shear-force topography shows terrace-like protrusions rising up to a height of 42 nm. Each plateau has a height of roughly 6 nm. In image (*b*) regions of high fluorescence directly correlate with multistacks in the topography, apart from some protrusions in the lower left part that are considered to be a preparation artifact. It is important to emphasize that the direct comparison of the two images allows for an unambiguous assignment whether excluded material contains protein or not. The crosses indicate locations that were used for a quantitative evaluation presented in Fig. 6. Excitation power, 3.8 nW; background fluorescence, 2.7 ± 0.6 kc/s; pixel integration time, 19 ms.

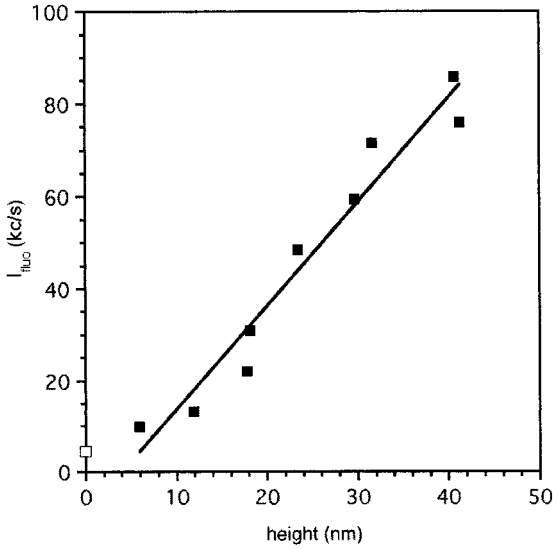

FIGURE 6 Relation between fluorecence intensity and height of the multilamellar exclusions (data extracted from Fig. 5). Note that the measured heights are roughly multiples of 6 nm, i.e., the height of one lamella. The increase of the fluorescence with the height of the multilayer stacks seems to be linear. This suggests the same protein density in each lamella of the multilayer.

of every new lamella is accompanied by the same number of proteins per unit area.

Fig. 5 was chosen not only for the clear appearance of the fluorescent protrusions, but also because it shows a second type of some rarely occurring protrusions that contain no fluorescence (Fig. 5 *a*, *bottom left*). The existence of the two different types of protrusions proves that the optical and the topographical contrast are independent of each other in the images shown here. In fact, a possible cross-talk between the sample topology and the optical image is an important concern in SNOM and has been the reason for false interpretation in the past (Hecht et al., 1997).

The nonfluorescent protrusions are clearly an artifact caused by the film transfer from the air/water interface to the glass substrate. They do not occur when mica is used instead of glass, probably because the former is more regularly hydrophilic. They are consistently lower (4–5 nm) than the fluorescent protrusions and are most probably a simple lipid collapse phase. Furthermore, they can be translocated by an SFM tip during a scan with high load. This is in contrast to the fluorescent protrusions, which appeared to be anchored in the monolayer.

DISCUSSION

The aim of this study is a better understanding of the exclusion and reinsertion process of lung surfactant material on a molecular level. Because a substantial role in this process is ascribed to the SP-C, we explored its distribution within a model lung surfactant film. The SNOM technique used for this allowed simultaneous fluorescence and topography imaging. This proved to be a striking advantage over far-field light microscopy or SFM alone, respectively. Considering, for instance, the strongly fluorescing protein domains in Figs. 2 *b* and 4 *b*, a fluorescence image alone would not reveal whether the high intensity is due to a high local surface density of dyes in the monolayer or the formation of three-dimensional aggregates. Using the simultaneously acquired topographical image, it becomes unambiguously evident that below the equilibrium film pressure (Fig. 2 *b*) no protrusions are present. Other benefits of the applied technique are an optical resolution beyond the diffraction limit (180 nm for this work), the sensitive detection of fluorescence photons, and the reduced bleaching rate because of the low excitation intensity and short exposure time. Taken together, these advantages may explain the pronounced contrast in the protein-containing phase in Fig. 2 that has not been observed with conventional optical microscopy before. It should be noted here that SNOM may still need to be complemented by conventional SFM. This is because the topographical image obtained in a SNOM is usually of inferior quality to a conventional SFM image (for a comparison see Figs. 2 *a* and 3 *a*, respectively).

For the understanding of the exclusion process, the arrangement of the SP-C within the monolayer before the formation of the multilamellar phase provides valuable information. The protein is excluded from the liquid condensed (LC) phase into the LE phase. This is explained by the exclusion of bulky molecules from a condensed phase commonly observed. Within the liquid expanded (LE) phase, we observed two different regions. There are patches of high protein density with sharp edges, surrounded by a region of lower density, that exhibit a gradient toward the neighboring LC phase. The occurrence of a density gradient may be due to the high compression speed with respect to the characteristic time of demixing; an equilibrium between the LE and LC phase may not be reached, so that the intermediate region results. The distinct patches with the highest protein concentration may be the starting point from where the protrusions arise upon compression.

For an understanding of the exclusion process, it appears important to locate the SP-C also after the protrusions have formed. The corresponding micrographs of film B (Figs. 4 and 5) confirm our earlier assumption that the exclusion process is directly driven by the presence of the protein. It is found only within the multilayer stacks and in their close proximity. It appears that the SP-C from the monolayer is incorporated in the protrusions when they form, such that the process comes to an end, when all of the SP-C has left the monolayer. Hence, in the state of the film we observed here the monolayer still provides a reservoir of proteins for further protrusions. The intensity of the monolayer fluorescence of film B (0.44 kc/[s·nW], from Fig. 4 *b*), compared to that of film A suggests that this reservoir corresponds to the low density regions of the LE phase (0.68 kc/[s·nW],

from Fig. 2 *b*), rather than the high density region (1.89 kc/[s·nW], from Fig. 2 *b*). Comparing the fluorescence data of two different images is delicate. Here we have normalized by excitation intensity but not taken into consideration the different pixel step size (PSS), which influences the bleaching behavior ($PSS_{Fig.\ 2} = 78$ nm, $PSS_{Fig.\ 4} = 63$ nm). The smaller the PSS at a given pixel frequency, the higher the bleaching effect, which could explain the lower fluorescence value of film B compared to film A.

Focusing on the protrusions, a correlation between height and fluorescence intensity provides new insight with respect to their composition. The linear increase of the fluorescence with height suggests that the squeeze out of every lamella is accompanied by the same number of proteins per unit area. This is indicative of a process where one protein together with a fixed number of lipid molecules, most probably acting as a cooperative unit, is expelled from the monolayer surface. A comparison of the fluorescence of one double-layer lamella (3.5 kc/[s·nW]) with the fluorescence intensity of the bright domains in film A reveals a lower value for the intensity of film A (1.89 kc/[s·nW]). This can be attributed to the doubling of the protein content per unit area when the monolayer is transferred to a double layer. We have normalized by excitation intensity, but not taken into account the above-mentioned PSS ($PSS_{Fig.\ 5} = 25$ nm, $PSS_{Fig.\ 2} = 78$ nm). Both intensities could be higher, $I_{Fig.\ 5}$ because of the low PSS (enhanced bleaching), and $I_{Fig.\ 2}$ because of the high packing density (quenching).

In conclusion, the exclusion process is based on a protein-mediated structural change of the film. The formation of the multilamellar structures originates from lipid-protein interaction. In the bilayer, the α-helix of the protein most probably spans the hydrophobic moiety of the lipids, whereas the hydrophilic amino acid residues interact with lipid headgroups of the same and the neighboring bilayers (Fig. 7). The molecular arrangement of the lipid-protein complex in the monolayer is less evident, however. The interaction of the protein with the lipids might be better understood by solving its molecular orientation in the film at various pressure states. This was not revealed by the SNOM work presented here. However, measurements with polarization detection of the fluorescence emitted from a dye molecule in principle allows for determination of the dye's dipole orientation perpendicular to the optical axis (Bopp et al., 1996; Ruiter et al., 1997; Schütz et al., 1997). In this context, polarization measurement in this experiment might be profitable, too.

CONCLUSION

In order to better understand the biophysical properties of the lung surfactant, we focused on the role of one important component, the surfactant-associated protein C. It was previously demonstrated that SP-C promotes the formation of multiple lipid layers when the film is further compressed after it has reached the equilibrium surface pressure. Using fluorescence near-field microscopy, we demonstrated that these layers also contain the protein, as was previously assumed. Quantitative measurements suggest that each lamella in these stacks possesses the same protein density. Furthermore, when the film was kept below the equilibrium surface pressure, the SNOM permitted qualitative measurements of the partition of the SP-C into different phases of the monolayer at domain boundaries. We found pronounced protein density variations when the film was kept below the pressure where protrusions form. Coexisting with a pure lipid phase in the LC state, the LE phase was built up of two zones with different protein concentration. We assume the phase richest in protein to be the initiator for the later

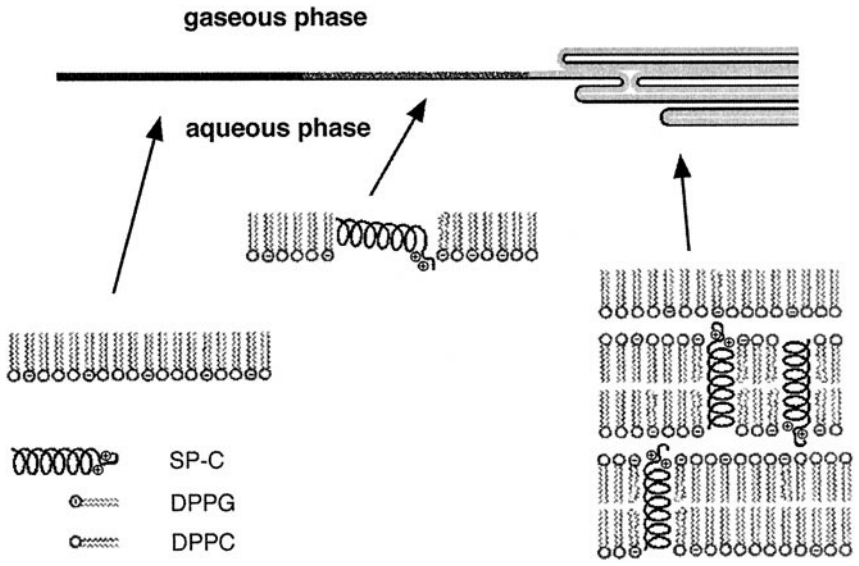

FIGURE 7 Molecular structure scheme of the lung surfactant model film at the air/water interface.

squeeze-out of film material. As an outlook, we suggest SNOM studies of lung surfactant films to be performed directly at the water/air interface. SNOM at the air/water interface has been shown to be very attractive (Kramer et al., 1998) and will provide additional information on domain formation, phase separation in the submicrometer range and squeeze out of material in situ.

We are grateful to A. Thess for SFM measurements and benefiting discussions as well as to Spectra Physics (Dr. A. Krüger) for the loan of the UV laser at moderate conditions. The Deutsche Forschungsgemeinschaft is acknowledged for financial support (SFB-266 B4).

REFERENCES

Amrein, M., A. von Nahmen, and M. Sieber. 1997. A scanning force- and fluorescence light microscopy study of the structure and function of a model pulmonary surfactant. *Eur. Biophys. J.* 26:349–357.

Betzig, E., J. K. Trautmann, T. D. Harris, J. S. Weiner, and R. L. Kostelak. 1991. Breaking the diffraction barrier: optical microscopy on a nanometer scale. *Science.* 251:1468–1470.

Bopp, M. A., A. J. Meixner, G. Tarrach, I. Zschokke-Granacher, and L. Novotny. 1996. Direct imaging single molecule diffusion in a solid polymer host. *Chem. Phys. Lett.* 263:721–726.

Galla, H.-J., N. Bourdos, A. von Nahmen, M. Amrein, and M. Sieber. 1998. The role of pulmonary surfactant protein C during the breathing cycle. *Thin Solid Films.* 327–329:632–635.

Hecht, B., H. Bielefeldt, Y. Inouye, D. W. Pohl, and L. Novotny. 1997. Facts and artifacts in near-field optical microscopy. *J. Appl. Phys.* 81:2492–2498.

Karrai, K., and R. D. Grober. 1995. Piezoelectric tip-sample distance control for near-field optical microscopes. *Appl. Phys. Lett.* 66: 1842–1844.

Kramer, A., T. Hartmann, R. Eschrich, and R. Guckenberger. 1998. Scanning near-field fluorescence microscopy of thin organic films at the water/air interface. *Ultramicroscopy.* 71:123–132.

Perez-Gil, J., K. Nag, S. Taneva, and K. M. W. Keough. 1992. Pulmonary surfactant protein SP-C causes packing rearrangements of dipalmitoylphosphatidylcholine in spread monolayers. *Biophys. J.* 63:197–204.

Ruiter, A. G. T., J. A. Veerman, M. F. Garciaparajo, and N. F. Vanhulst. 1997. Single-molecule rotational and translational diffusion observed by near-field scanning optical microscopy. *J. Phys. Chem. A.* 101: 7318–7323.

Schütz, G. J., H. Schindler, and T. Schmidt. 1997. Imaging single-molecule dichroism. *Optics Lett.* 22:651–653.

von Nahmen, A., M. Schenk, M. Sieber, and M. Amrein. 1997a. the structure of a model pulmonary surfactant as revealed by scanning force microscopy. *Biophys. J.* 72:463–469.

von Nahmen, A., A. Post, H.-J. Galla, and M. Sieber. 1997b. The phase behavior of lipid monolayers containing pulmonary surfactant protein C studied by fluorescence light microscopy. *Eur. Biophys. J.* 26:359–369.